Dalton Transactions

Accepted Manuscript

This is an *Accepted Manuscript*, which has been through the Royal Society of Chemistry peer review process and has been accepted for publication.

Accepted Manuscripts are published online shortly after acceptance, before technical editing, formatting and proof reading. Using this free service, authors can make their results available to the community, in citable form, before we publish the edited article. We will replace this *Accepted Manuscript* with the edited and formatted *Advance Article* as soon as it is available.

You can find more information about *Accepted Manuscripts* in the Information for Authors.

ROYAL SOCIETY OF CHEMISTRY

www.rsc.org/dalton

Journal Name
Dalton Transactions
Dynamic Article Links ►

Cite this: DOI: 10.1039/c0xx00000x

www.rsc.org/xxxxxx

ARTICLE TYPE

Electronic excited states of chromium and vanadium bisarene complexes revisited: Interpretation of the absorption spectra on the basis of TD DFT calculations

Sergey Ketkov,*[a,b] Nikolai Isachenkov[a], Elena Rychagova[a,b] and Wen-Bih Tzeng[c]

Received (in XXX, XXX) Xth XXXXXXXXX 20XX, Accepted Xth XXXXXXXXX 20XX
DOI: 10.1039/b000000x

The nature and energies of the $(Arene)_2Cr$, $(Arene)_2V$ and $(Arene)_2Cr^+$ (Arene = η^6-C_6H_6, η^6-C_6H_5Me, η^6-1,3-$C_6H_4Me_2$, and η^6-1,3,5-$C_6H_3Me_3$) electronic excited states have been determined on the basis of the time-dependent density functional theory (TD DFT) approach and comparison with the gas-phase and condensed-phase absorption spectra. Both valence-shell and Rydberg electronic excitations were taken into account. The TD DFT results appear to describe correctly the influence of the metal atom and the ligand on the band positions and intensities in the UV-visible absorption spectra as well as the mixing of Rydberg and intravalency states. The TD DFT calculations suggest new assignments for long-wavelength valence-shell absorption bands in the spectra of $(Arene)_2V$ and $(Arene)_2Cr^+$.

Introduction

Over half a century transition metal bisarene complexes, similar to metallocenes, have been playing a key role in both fundamental and applied coordination chemistry. On the one hand, studies of their electronic structures with a wide number of theoretical and experimental approaches form a basis for understanding the nature of metal-ligand delocalised chemical bonds.[1] On the other hand, considerable interest has been focused on the metal arene derivatives during past decades because of their relevance for organic synthesis, catalysis, molecular sensors, magnetic materials, spintronic devices and metal-containing polymers.[1-6] In particular, the organometallic sandwich clusters $(Bz_{n+1})M_n$ containing metal atoms (M) and η^6-C_6H_6 benzene molecules (Bz) as well as the $(BzM)_\infty$ one-dimensional polymers (molecular wires) have recently attracted increased attention due to their unusual electronic and magnetic properties.[6-11] Their electronic structures were studied intensely with use of photoelectron spectroscopy[12-14] and quantum chemistry.[15-20]

To predict optical properties of such systems, reliable information on the nature and energies of electronic excited states of the parent bisbenzene complexes $(Bz)_2M$ and their substituted derivatives is of extreme importance. However, interpretations of the $(Bz)_2M$ electronic absorption spectra appear to be incomplete and contradictory. The condensed-phase spectra are usually assigned on the basis of the qualitative valence-shell MO diagram[21] (Fig. 1) describing the $Bz_2 \rightarrow M$ electron donation (e_{1g} and e_{1u} orbitals in the D_{6h} point group) and the $M \rightarrow Bz_2$ back donation (e_{2g} orbitals) on the formation of the sandwich molecule.

The UV and visible spectra of the "18-electron" $(Bz)_2Cr$[22-28] (the ground-state electronic configuration $\ldots[1e_{2g}]^4[1a_{1g}]^2$) and "17-electron" $(Bz)_2V$[27-30] ($\ldots[1e_{2g}]^4[1a_{1g}]^1$) neutral sandwiches in organic solvents reveal very weak long-wavelength absorption features A, D (Table 1) in the 600-800 nm region, stronger bands B, E at 400-500 nm and very intense peaks C, F at 310-320 nm. The spectrum of the "17-electron" $(Bz)_2Cr^+$ ion[22] shows a broad weak band G in the near IR region and two strong peaks H and I at 334 and 273 nm, respectively.

The A, D and G weak features were assigned on the basis of ligand field theory[26] and multiple scattering SCF-X_α calculations[29,31] to the symmetry forbidden d-d transitions involving the $1e_{2g}$, $1a_{1g}$ and $2e_{1g}$ MOs (Fig.1, Table 1). Shoulder B was attributed to the forbidden d-d and metal-to-ligand charge transfer (MLCT) excitations. Peak E in the spectrum of $(Bz)_2V$ had initially been interpreted[29] with use of X_α MO calculations as the d-d and MLCT transitions originating at the $1a_{1g}$ MO but later it has been reassigned[30] to the allowed $1e_{1u} \rightarrow 1a_{1g}$ LMCT because of a red shift on methylation of the benzene rings. The E assignment to the transitions from the $1a_{1g}$ MO does not agree with the presence of a similar peak in the spectrum of $(Bz)_2Ti$[32] possessing a vacant $1a_{1g}$ orbital. The $1e_{1u} \rightarrow 1a_{1g}$ LMCT was suggested[31] to be responsible also for the intense H peak in the $(Bz)_2Cr^+$ spectrum. Strong bands C, F and I were attributed[29, 31] to the allowed $1e_{2g} \rightarrow 1e_{2u}$ MLCT transitions on the basis of energies derived from the X_α MO calculations. However, the red shift of the F peak on methylation of $(Bz)_2V$ was a reason for its assignment to the $1e_{1u} \rightarrow 1e_{1g}$ LMCT with an opposite direction of the charge transfer.[30] Since bands C and I also shift to longer wavelength on introduction of alkyl groups,[27,28] the latter interpretation should be taken into account for these absorption features.

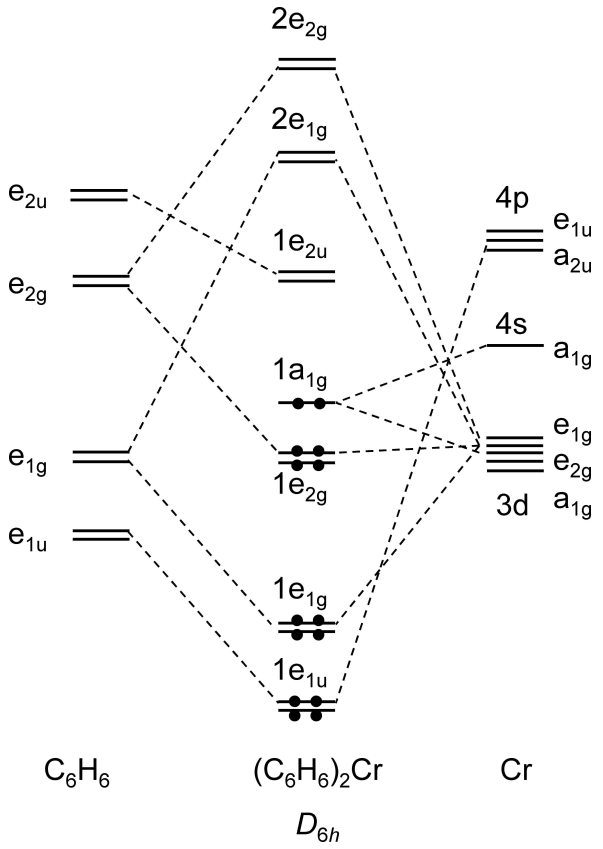

Fig. 1. Qualitative MO diagram of $(Bz)_2Cr$ in the D_{6h} point group.

Table 1. Energies E (eV), molar extinction ε ($M^{-1}cm^{-1}$) and earlier assignments corresponding to the absorption bands observed in the solution spectra[22-30] of the "18-electron" and "17-electron" bisbenzene complexes $(Bz)_2M$ (M = Cr, V, Cr^+).

M	Band	E	ε	Assignments[a]	Ref.
Cr	A	1.86[b]	25	d-d; $1a_{1g}\rightarrow 2e_{1g}$ (F)	31
	B	3.08[b]	800	d-d, MLCT; $1a_{1g}\rightarrow 2e_{1g}$ $+1a_{1g}\rightarrow 1e_{2u}$ (F)	31
	C	4.00	8000	MLCT; $1e_{2g}\rightarrow 1e_{2u}$ (A)	31
V	D	1.61 1.81[b]	50 30	d-d; $1a_{1g}\rightarrow 2e_{1g}$ (F)	30
	E	2.79	1800	LMCT; $1e_{1u}\rightarrow 1a_{1g}$ d-d, MLCT; $1a_{1g}\rightarrow 1e_{2u}$ $+ 1a_{1g}\rightarrow 2e_{1g}+ 1a_{1g}\rightarrow 2e_{2g}$ (F)	30 29
	F	3.87	15000	LMCT; $1e_{1u}\rightarrow 2e_{1g}$ (A) MLCT; $1e_{2g}\rightarrow 1e_{2u}$ (A)	30 29
Cr^+	G	1.05	10	d-d; $1e_{2g}\rightarrow 2e_{1g}$ (F) d-d; $1a_{1g}\rightarrow 2e_{1g}$ (F) d-d; $1e_{2g} \rightarrow 1a_{1g}$ (F)	23 24 25, 31
	H	3.71	6000	LMCT; $1e_{1u}\rightarrow 1a_{1g}$ (A) MLCT LMCT	31 22 23
	I	4.54	6000	MLCT; $1e_{2g}\rightarrow 1e_{2u}$ (A) MLCT LMCT	31 22 23

[a] The MO notations correspond to those in Fig.1; A- allowed, F-forbidden transitions.

[b] Shoulder.

These numerous discrepancies in the interpretations of the valence-shell absorption spectra of chromium and vanadium bisbenzene complexes prompt us to undertake a computational study of $(Bz)_2Cr$, $(Bz)_2V$, $(Bz)_2Cr^+$ and their methylated derivatives with use of recently developed time dependent density functional theory.[33] This approach showed a good agreement with experiment for various metal complexes[34-36] including closely related metallocenes.[37-39]

On the other hand, the gas-phase electronic absorption spectra of chromium and vanadium bisarene complexes reveal clearly defined Rydberg transitions originating at the non-bonding $1a_{1g}$ orbital that represents an almost "pure" $3d_{z}2$ level of the metal atom.[40-47] Rydberg bands form series converging at the ionization threshold. The series members are described by the well-known Rydberg formula

$$\nu_n = I - \mathbf{R} / (n - \delta)^2 = I - T,$$

where ν_n is the peak position, n - the principal quantum number, I - the ionization energy, **R** - the Rydberg constant (109737 cm^{-1}), δ - the quantum defect and T – the term value. Rydberg peaks disappear from the absorption spectra on going from the gas to the condensed phase because of diffuse character of Rydberg MOs.

Unambiguous assignments of these excitations have been made previously on the basis of the corresponding quantum defects, term values and vibronic structures as well as analysis of the changes in the Rydberg structures on going from $(Bz)_2Cr$ and $(Bz)_2V$ to their substituted derivatives.[40,41,43-47] The gas-phase absorption spectrum of $(Bz)_2Cr$ reveals the $Rnp_{x,y}$ and Rnp_z series. The lowest allowed Rydberg transition ($R4p_{x,y}$) corresponds to a strong narrow peak at 374 nm (3.32 eV). The first member of the Rnp_z series ($R4p_z$) is broadened beyond detection because of Rydberg/valence mixing.[43,46] The position of the unperturbed $R4p_z$ state can, however, be easily found on the basis of the $R4p_z$ term value obtained from the spectrum of isoelectronic $(\eta^7\text{-}C_7H_7)(\eta^5\text{-}C_5H_5)Cr$[48,49] ($T_{R4p_z}$ =15490 cm^{-1}). By analogy, the energy of the forbidden $1a_{1g}\rightarrow R4s$ transition, which is not observed in the $(Bz)_2Cr$ spectrum, can be determined from the experimental T_{R4s} = 21390 cm^{-1} value of $(\eta^7\text{-}C_7H_7)(\eta^5\text{-}C_5H_5)Cr$.[48,49] The resulting energies of the $(Bz)_2Cr$ R4s and $R4p_z$ states are, respectively, 2.78 and 3.55 eV.

Rydberg parameters of the gas-phase sandwich molecules provide a powerful instrument to verify the results of quantum chemistry. We decided, therefore, to perform TD DFT calculations for the $(Arene)_2Cr$, $(Arene)_2V$ and $(Arene)_2Cr^+$ systems (Arene = Bz, $\eta^6\text{-}C_6H_5Me$ (Tol), $\eta^6\text{-}1,3\text{-}C_6H_4Me_2$ (Xyl) and $\eta^6\text{-}1,3,5\text{-}C_6H_3Me_3$ (Mes)) taking into account both intravalency and lower-lying Rydberg R4s, R4p transitions. In the earlier TD DFT studies of $(Bz)_2Cr$[37] and $(Bz)_2V$[20] the calculated transition energies were not compared with the interpreted experimental gas-phase absorption spectra[40-43] so no definite assignments could be made. The results obtained in this work appear to describe correctly the influence of the metal atom and the ligand on the band positions and intensities in the UV-visible absorption spectra as well as the relative energies and mixing of the Rydberg and intravalency electronic excited states. The TD

DFT data provide new assignments for valence-shell absorption bands in the spectra of $(Arene)_2V$ and $(Arene)_2Cr^+$.

Computational details

The calculations were carried out with the Gaussian 09 program package.[50] For the $(Bz)_2Cr$ molecule, the geometry optimization and subsequent TD DFT procedure were performed using the HCTH147,[51] B3PW91[52] and B3LYP[53] functionals together with the "double-ζ" and "triple-ζ" quality basis sets[54] (6-31G(d,p), 6-31++G(d,p), 6-311++G(d,p), TZVP). The optimized molecular geometries correlate very well with the X-Ray and electron diffraction data.[55] Comparison of the computed electronic state energies with the experimental parameters of bands A, C (Table 1) and Rydberg transitions R4s, R4p[43,46] showed that the B3LYP/6-31++G(d,p) level of theory provided a good agreement with the experiment despite lower computational costs. This level was used then for the TD DFT calculations of other bisarene systems. Among the conformers of the toluene and *m*-xylene derivatives, the C_{2h} rotational isomers with opposite locations of the Me groups in the two rings were chosen for our calculations. The mesitylene complexes with the staggered conformation of the methyl substituents (the D_{3d} point group) were investigated. The number of states included in the TD DFT procedure was 60-120, depending on the molecule studied. This large number of excited levels was taken to reach the states of interest (e.g. the $1e_{1u}\rightarrow 1a_{1g}$ transition in $(Bz)_2V$ corresponds to the state number 103). The highest excited-state energy achieved was 7.5 eV but our interest was focused on the lower-lying electronic levels with energies below 5 eV.

Results and discussion

$(Arene)_2Cr$

The ground-state $(Bz)_2Cr$ DFT calculations at various levels of theory have been reported earlier.[21,56,57] Our previous study[57] of the vibrational frequencies and ionization energy of this molecule demonstrated that the parameters obtained with the BPW91/TZVP and B3PW91/TZVP combinations of the functional and basis set are very close to the experimental values. However, when computing the excited state energies, TD DFT at the B3PW91/TZVP level appears to overestimate the Rydberg R4p energies by ~2 eV (See Supporting Information, Fig.S1.). On the other hand, the HCTH147/TZVP and HCTH147/6-311++G(d,p) calculations provide, respectively, too large (1.15 eV) and too small (0.26 eV) R4s-R4p state separations as compared to the experimental value of 0.55 eV. These shifts lead to a change in the relative energies of the intravalency and Rydberg transitions and result in an incorrect scheme of the Rydberg/valence mixing. The best agreement between the theoretical and experimental state separations corresponding to both A, C valence-shell absorption bands[22-28] and R4s, R4p Rydberg transitions[43,46] was achieved at the B3LYP/6-311++G(d,p) and B3LYP/6-31++G(d,p) levels of TD DFT (See Supporting Information, Fig.S1.). We used, therefore, the latter combination of the functional and basis set to analyse the MO and excited states of $(Tol)_2Cr$, $(Xyl)_2Cr$ and $(Mes)_2Cr$. This level of theory appeared to provide good agreement with the experiment for the excited states of transition-metal chelate complexes.[35]

The B3LYP/6-31++G(d,p) quantitative MO diagram of $(Bz)_2Cr$ (Fig.2) shows that the higher occupied orbitals correspond to those in Fig.1. However, the $2a_{1g}$ LUMO represents the lowest Rydberg s orbital (R4s). The next vacant level is valence-shell $1e_{2u}$. The 4p and 4d Rydberg orbitals lie between the $1e_{2u}$ and $2e_{2g}$ intravalency levels. The Rydberg MOs are easily distinguished from the valence shell orbitals due to their diffuse isosurfaces (Fig. 2). The MO diagrams for the methylated complexes are similar to that or $(Bz)_2Cr$ though some orbitals are mixed due to the molecular symmetry reduction. For simplicity, we retain the D_{6h} group notations for MOs and electronic states of the substituted molecules. Our TD DFT calculations confirm that the lowest Rydberg excitations originating at the $1a_{1g}$ and $1e_{2g}$ orbitals lie below the intense allowed $^1A_{1g}\rightarrow{}^1A_{2u}$ component of the $1e_{2g}\rightarrow 1e_{2u}$ transition corresponding to band C. It has been demonstrated previously[40-46] that the Rydberg transitions involving the bonding $1e_{2g}$ orbital are broadened beyond detection so we consider only Rydberg excitations of the $1a_{1g}$ electron when verifying the TD DFT results.

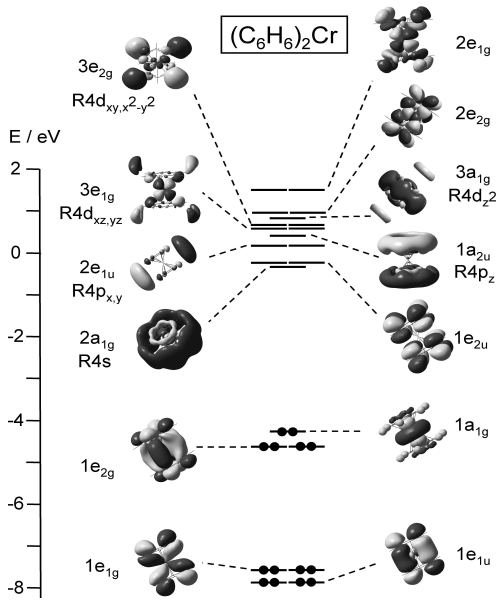

Fig.2. B3LYP/6-31++G(d,p) quantitative energy diagram and isosurfaces of the $(Bz)_2Cr$ orbitals. The valence-shell MO notations correspond to those in the qualitative scheme (Fig. 1).

The B3LYP/6-31++G(d,p) energies of the $(Arene)_2Cr$ excited states (Table 2) are 0.3-0.5 eV higher than those derived from the absorption spectra. Nevertheless, the calculated distances between the excited levels and the picture of configuration interactions agree very well with the experiment. The lowest singlet excited state corresponds to the forbidden $1a_{1g}\rightarrow 2e_{1g}$ d-d transition mixed with the $1a_{1g}\rightarrow 3e_{1g}$ Rydberg $R4d_{xz,yz}$ excitation. The A shoulder in the solution-phase absorption spectra of $(Arene)_2Cr$ should be assigned to the valence-shell d-d component which agrees well with the previous interpretation.[31] The $(Bz)_2Cr$ first triplet state with a $(\ldots[1e_{2g}]^4[1a_{1g}]^1[2e_{1g}]^1)$ configuration (1.33 eV above the ground singlet state) can also contribute to feature A.

Numerous valence-shell and Rydberg transitions lie between

the excitations responsible for bands A and C. The $(Bz)_2Cr$ $^1A_{2u}$ state corresponding to band C is the excited level No. 31. Feature B in the $(Arene)_2Cr$ solution spectra can be assigned to the $^1A_{1g}\rightarrow{}^1A_{1u}$ and $^1A_{1g}\rightarrow{}^1E_{2u}$ components of the $1e_{2g}\rightarrow 1e_{2u}$ transition lying at 3.0-3.3 eV (Table 2). These components are symmetry forbidden for $(Bz)_2Cr$ but they become allowed for its methylated derivatives. Correspondingly, low but non-zero oscillator strengths were obtained for the Tol, Xyl and Mes complexes (Table 2). Band B can also be contributed by the intravalency excitations from MO $1e_{2g}$ to MOs $2e_{2g}$ and $2e_{1g}$ (Fig. 2) with the calculated energies of 3.3-3.6 eV. They are symmetry forbidden for the molecules possessing a centre of symmetry so intensity can be borrowed from the strong $1e_{2g}\rightarrow 1e_{2u}$ component as a result of vibronic interactions.

Table 2. TD DFT[a] / experimental[22-28] energies (eV) of selected $(Arene)_2Cr$ electronic states and the corresponding MO transitions.

State	Transition	$(Bz)_2Cr$	$(Tol)_2Cr$	$(Xyl)_2Cr$	$(Mes)_2Cr$
$^1E_{1g}$	$1a_{1g}\rightarrow 2e_{1g}$ d-d, MLCT, $1a_{1g}\rightarrow 3e_{1g}$ $R4d_{xz,yz}$	2.32(0.000)/ 1.86	2.33[b](0.000)/ 1.86	2.31[b](0.000)/ 1.86	2.33(0.000)/ 1.74
$^1A_{1g}$	$1a_{1g}\rightarrow 2a_{1g}$ R4s	3.29(0.000)/ 2.78	3.22(0.000)/ 2.84	3.15(0.000)/ 2.79	3.07(0.000)/ 2.77
$^1A_{1u}+{}^1E_{2u}$	$1e_{2g}\rightarrow 1e_{2u}$ MLCT	3.32[b](0.000)/ 3.08	3.26[b](0.001)/ 3.03	3.18[b](0.001)/ 3.03	3.06[b](0.001)/ 2.78
$^1E_{1u}$	$1a_{1g}\rightarrow 1e_{1u}$ $R4p_{x,y}$	3.78(0.064)/ 3.32	3.63[b](0.030)/ 3.17	3.52[b](0.083)/ 3.07[b]	3.47(0.001)/[d]
$^1A_{2u}$	$1a_{1g}\rightarrow 1a_{2u}$ $R4p_z$,[c] $1e_{2g}\rightarrow 1e_{2u}$ MLCT	4.01(0.000)/ 3.55[d]	3.96(0.036)/[d]	3.84[e](0.031)/ 3.30	3.66(0.001)/[d]
$^1A_{2u}$	$1e_{2g}\rightarrow 1e_{2u}$ MLCT,[c] $1a_{1g}\rightarrow 1a_{2u}$ $R4p_z$	4.52(0.516)/ 4.00	4.46[b](0.523)/ 3.83	4.32[b](0.483)/ 3.73	4.21[b](0.441) 3.58

[a] The calculated oscillator strengths are given in parentheses.

[b] An averaged energy and a sum of oscillator strengths is given for the components arising from state splitting.

[c] The main component of the excitation.

[d] Non-observable.

[e] For $(Xyl)_2Cr$, the $R4p_z$ state is mixed with the $R4p_y$ level instead of the MLCT state.

TD DFT predicts that the $R4p_{x,y}$ states of $(Arene)_2Cr$ are not mixed with the intravalency levels. Correspondingly, they are observed as sharp Rydberg peaks in the gas-phase absorption spectra of $(Bz)_2Cr$, $(Tol)_2Cr$ and $(Xyl)_2Cr$.[41,43,44] On going to the Mes complex the $R4p_{x,y}$ absorption band becomes undetectable. This change is explained by the calculated oscillator strength which is very low for $(Mes)_2Cr$ (Table 2). The ratio of the oscillator strengths in $(Bz)_2Cr$ and $(Mes)_2Cr$ is 64 which means that the $R4p_{x,y}$ band in the $(Mes)_2Cr$ spectrum is not observed because of its negligible intensity. In contrast to $R4p_{x,y}$, the $R4p_z$ state is predicted to mix with the $^1A_{2u}$ excited level arising from the $1e_{2g}\rightarrow 1e_{2u}$ transition. Indeed, the $R4p_z$ peak is broadened beyond detection in the spectra of $(Bz)_2Cr$, $(Tol)_2Cr$ and $(Mes)_2Cr$.[41,43,44] The $1a_{1g}\rightarrow R4p_z$ transition is observed as a shoulder in the spectrum of $(Xyl)_2Cr$ but in this case, according to our calculations, the $R4p_z$ state has an admixture of the Rydberg $4p_y$ level instead of the valence-shell state (Table 2).

TD DFT unambiguously assigns strong absorption band C in the $(Arene)_2Cr$ spectra to the allowed $^1A_{2u}$ component of the $1e_{2g}\rightarrow 1e_{2u}$ transition. This interpretation is in accord with the SCF-X_α calculations.[31] The B3LYP/6-31++G(d,p) TD DFT model provides, therefore, both perfect assignments of the absorption features observed in the spectra of $(Arene)_2Cr$ and explanations of the changes taking place on methylation of benzene rings. The successful employment of TD DFT to the "18-electron" chromium bisarene complexes prompts us to study more complicated open-shell "17-electron" systems.

$(Arene)_2V$

The unrestricted formalism leads to separate calculations of the α and β orbitals for the open-shell molecules. The MO diagram of $(Bz)_2V$ (Fig. 3) contains, therefore, two sets of orbitals. The energies of the occupied or vacant α and β MOs corresponding to each other are mostly similar but not the same. The largest energy difference takes place for the $1a_{1g}$ orbital which is occupied in the α-set and vacant in the β-set. The $(Bz)_2V$ MO scheme of vacant α-orbitals resembles that of $(Bz)_2Cr$ (Fig. 2). For the occupied α-MOs, an inversion of the $1e_{2g}$ and $1a_{1g}$ levels takes place (Fig.3). In the structure of the vacant β-orbitals, the $2a_{1g}$ MO raises up in energy as a result of an interaction with the $1a_{1g}$ level.

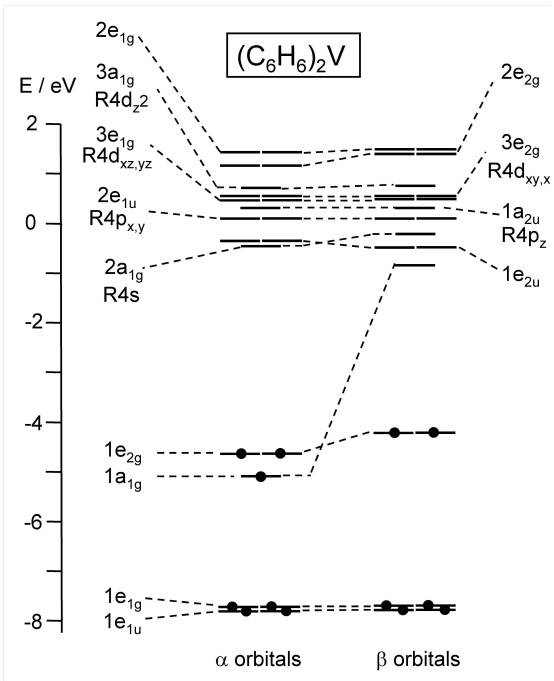

Fig.3. B3LYP/6-31++G(d,p) diagram of the $(Bz)_2V$ orbitals. The MO notation corresponds to that in $(Bz)_2Cr$.

Taking into account similar quantitative diagrams of the $(Bz)_2V$ vacant α-MOs and $(Bz)_2Cr$ unoccupied levels, one might expect similarity in the Rydberg structures for the two sandwich molecules. However, the $1a_{1g}$ α-orbital energy decreases on going from $(Bz)_2Cr$ to $(Bz)_2V$ (-0.73 eV at the B3LYP/6-31++G(d,p) level of theory), which correlates well with an increase in the $1a_{1g}$ ionization potential (0.76 eV[58] from the photoelectron spectra).

As a result, the Rydberg transitions originating at the $1a_{1g}$ orbital of $(Bz)_2V$ shift to blue as compared to those in $(Bz)_2Cr$. The $R4p_{x,y}$ peak in the $(Bz)_2V$ gas-phase spectrum is observed at 3.98 eV.[27,41,46] The TD DFT calculations reproduce nicely these changes.

Table 3. TD DFT[a] / experimental[29,30] energies (eV) of selected $(Arene)_2V$ electronic states and the corresponding MO transitions.

State	Transition	$(Bz)_2V$	$(Tol)_2V$	$(Xyl)_2V$	$(Mes)_2V$
$^2E_{2g}$	$1e_{2g}\rightarrow1a_{1g}$ d-d, MLCT	1.62[b](0.000)/ 1.71[b]	1.68[b](0.000)/ 1.60[b]	1.57[b](0.000)/ 1.61[b]	1.53[b](0.000)/ 1.62[b]
"$^4A_{2u}$"	$1e_{2g}\rightarrow1e_{2u}$ MLCT	2.46(0.012)/ 2.79	2.42(0.012)/ 2.73	2.37(0.012)/ 2.68	2.28(0.013)/ 2.64
"$^4A_{1u}$" + "$^4E_{2u}$"	$1e_{2g}\rightarrow1e_{2u}$ MLCT	3.05[b](0.000)/ 2.79	3.01[b](0.000)/ 2.73	2.93[b](0.001)/ 2.68	2.84[b](0.000)/ 2.64
$^2A_{1g}$	$1a_{1g}\rightarrow2a_{1g}$ R4s	3.99(0.000)/[d]	3.98(0.000)/[d]	3.92(0.000)/[d]	3.84(0.000)/[d]
"$^2A_{2u}$"	$1e_{2g}\rightarrow1e_{2u}$ MLCT	4.25(0.537)/ 3.87	4.17[b](0.503)/ 3.78	3.97[b](0.366)/ 3.68	3.86[b](0.419) 3.58
$^2E_{1u}$	$1a_{1g}\rightarrow1e_{1u}$ $R4p_{x,y}$	4.57(0.021)/ 3.98	4.41[b](0.011)/[d]	3.52[b](0.012)/[d]	4.24(0.000)/[d]
$^2A_{2u}$	$1a_{1g}\rightarrow1a_{2u}$ $R4p_z$	4.80(0.046)/ 4.22	4.69(0.026)/ 4.12	4.57/(0.012)/[d]	4.44(0.002)/[d]

[a] The calculated oscillator strengths are given in parentheses.

[b] An averaged energy and a sum of oscillator strengths is given for the components arising from state splitting.

[c] The main component of the excitation.

[d] Non-observable.

[e] For $(Xyl)_2Cr$, the $R4p_z$ state is mixed with the $R4p_y$ level instead of the MLCT state.

The calculated $R4p_{x,y}$ and $R4p_z$ state energies of $(Bz)_2V$ are, respectively, 0.11 and 0.35 eV higher that of the $1e_{2g}\rightarrow1e_{2u}$ A_{2u} component (Table 3). As a result, the $R4p_z$ state does not mix with the MLCT A_{2u} level. Indeed, the experimental gas-phase spectrum of $(Bz)_2V$[27,41,46] reveals both $R4p_{x,y}$ and $R4p_z$ transitions as narrow peaks at 3.98 and 4.22 eV, respectively. The experimental peak separation (0.24 eV) correlates well with the calculated energy difference (0.22 eV). On going to $(Mes)_2V$ the oscillator strengths of the R4p transitions decrease dramatically (Table 2). Accordingly, no R4p peaks are observed in the spectrum of the mesitylene complex.[27,41,46] The 4s Rydberg transition lies close to the intense intravalency $1e_{2g}\rightarrow1e_{2u}$ excitation. The R4s peak cannot be observed in the experimental spectra of the $(Bz)_2V$ substituted derivatives[27,41,46] because of its low intensity (Table 3).

The TD DFT results assign the strongest valence-shell band F in the spectra of $(Arene)_2V$ to the allowed component of the $1e_{2g}\rightarrow1e_{2u}$ MLCT transition. This is in agreement with the previous SCF-X_α calculations.[29] Such interpretation contradicts to the newer assignment of band F as the LMCT $1e_{1u}\rightarrow2e_{1g}$ transition[30] based on the red shift on methylation. However, the TD DFT energy of this LMCT excitation in $(Bz)_2V$ (5.87 eV) is too high to be associated with band F (3.87 eV). On the other hand, our calculations show that the $1e_{2g}\rightarrow1e_{2u}$ MLCT transition shifts to lower energies on going from $(Bz)_2V$ to its methylated derivatives in agreement with the experiment (Table 3).

The TD DFT computations reveal one more component of the $1e_{2g}\rightarrow1e_{2u}$ MLCT transition with a non-zero oscillator strength even for highly-symmetric $(Bz)_2V$. Its calculated energy (2.28-2.46 eV, Table 3) is appropriate to associate this excitation with the E band in the spectra of $(Arene)_2V$ (Table 1). The appearance of the additional $1e_{2g}\rightarrow1e_{2u}$ components arises from the unrestricted formalism employed for calculations of the open-shell systems. The α and β orbitals have different energies so configurations $\ldots[\alpha1e_{2g}]^2[\alpha1a_{1g}]^1\ldots[\beta1e_{2g}]^1[\beta1e_{2u}]^1$ and $\ldots[\alpha1e_{2g}]^1[\alpha1a_{1g}]^1[\alpha1e_{2u}]^1\ldots[\beta1e_{2g}]^2$ describing the MLCT state are not equivalent. As a result, instead of one $e_{2g}\otimes e_{2u} = A_{1u}+A_{2u}+E_{2u}$ set of excited states, TD DFT produces two such sets for the $1e_{2g}\rightarrow1e_{2u}$ transition in $(Bz)_2V$ (Fig. 4). For the lower-lying set, the $\langle S^2\rangle$ expectation values are 2.3-2.7. This is indicative of significant quartet-state contaminations ($\langle S^2\rangle = 0.75$ and $\langle S^2\rangle = 3.75$ for "pure" doublet and quartet states, respectively). Primitively, the lower-lying set of states can be considered as being derived from the doublet-quartet transitions while the higher-energy set is formed by doublet-doublet excitations. Spin-orbit coupling mixes the states of one type belonging to the two sets. Then the $^2A_{1g} \rightarrow$ "$^4A_{2u}$" transition borrows intensity from the allowed $^2A_{1g} \rightarrow$ "$^2A_{2u}$" excitation.

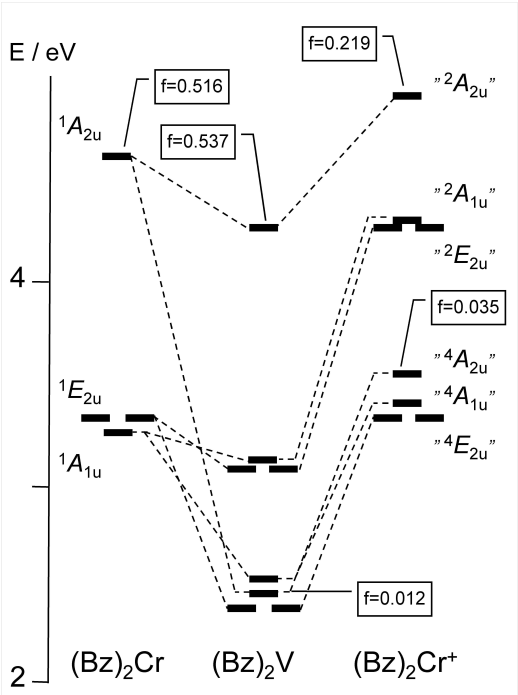

Fig.4. Excited states resulting from the $1e_{2g}\rightarrow1e_{2u}$ transition in bisbenzene complexes. Non-zero oscillator strengths f calculated at the B3LYP/6-31++G(d,p) level of TD DFT are indicated.

Alternatively, the increase in the number of the $1e_{2g}\rightarrow1e_{2u}$ allowed components on going from $(Bz)_2Cr$ to $(Bz)_2V$ can be explained if we consider spin-orbit interactions within the doublet-state manifold. In the D_{6h} point group, the spin wavefunction belongs to the A_{1g} irreducible representation for singlet states and to the $E_{1/2g}$ type for doublet states[59] (the double

point group is required for the S=1/2 systems). The spin wavefunction does not change, therefore the irreducible representations of singlet states, and the $1e_{2g}\rightarrow 1e_{2u}$ transition in $(Bz)_2Cr$ produces the $e_{2g}\otimes e_{2u} = A_{1u}+A_{2u}+E_{2u}$ levels, the excitation to the A_{2u} state being allowed by the selection rules. However, the spin-orbit coupling in the doublet $(Bz)_2V$ leads to a change of the ground-state type from $^2A_{1g}$ to $E_{1/2g}$ and the types of the $1e_{2g}\rightarrow 1e_{2u}$ excited states from $^2A_{1u}+^2A_{2u}+^2E_{2u}$ to $E_{1/2u}+E_{1/2u}+E_{3/2u}+E_{5/2u}$. The $E_{1/2g}\rightarrow E_{1/2u}$ and $E_{1/2g}\rightarrow E_{3/2u}$ transitions are symmetry allowed in the D_{6h} double point group so for $(Bz)_2V$ we have three allowed states instead of one.

Band E in the spectrum of $(Bz)_2V$ can, therefore, be assigned to the $^2A_{1g} \rightarrow$ "$^4A_{2u}$" transition with the calculated oscillator strength of 0.012 or to the excitations terminating at the $E_{1/2}$ and $E_{3/2}$ states derived from the "$^2A_{1u}$" and "$^2E_{2u}$" components of the $1e_{2g}\rightarrow 1e_{2u}$ transition. Since a similar peak is observed in the spectrum of singlet $(Bz)_2Ti$,[32] it is possible that vibronic interactions also provide mechanisms for borrowing intensity from the strong $1e_{2g}\rightarrow 1e_{2u}$ component.

TD DFT testifies against the assignment[30] of the E band to the $1e_{1u}\rightarrow 1a_{1g}$ LMCT excitation. The B3LYP/6-31++G(d,p) energy of this transition in $(Bz)_2V$ (5.62 eV) exceeds dramatically the experimental value corresponding to peak E (2.79 eV).[30] The red shift of the E peak on methylation[30] agrees with the interpretation suggested in this work since the TD DFT energies of the longer-wavelength component of the $1e_{2g}\rightarrow 1e_{2u}$ transition decrease on going from $(Bz)_2V$ to $(Mes)_2V$ (Table 3).

The weak D band in the spectra of $(Arene)_2V$ can be assigned on the basis of our TD DFT results to the forbidden $1e_{2g}\rightarrow 1a_{1g}$ excitation. The interpretation of this feature as the $1a_{1g}\rightarrow 2e_{1g}$. transition[30] seems to be less preferable since the TD DFT energy of the corresponding $^2E_{1g}$ state in $(Bz)_2V$ is 2.72 eV which is 1.01 eV higher than the experimental value. The D assignment to a transition terminating at the $1a_{1g}$ orbital is supported by analysis of excited states of the isoelectronic $(Arene)_2Cr^+$ ions.

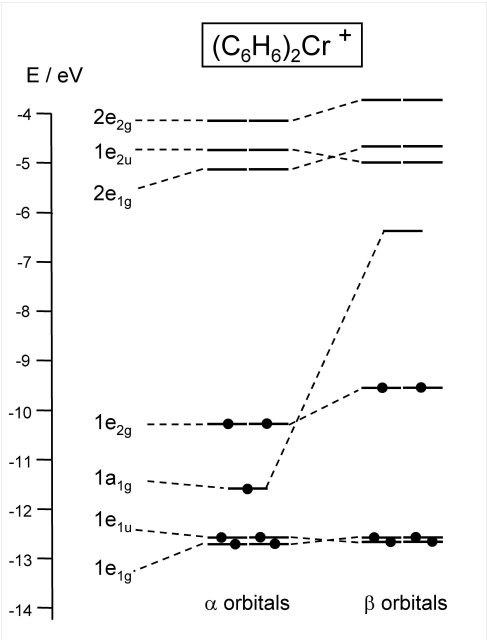

Fig.5. B3LYP/6-31++G(d,p) scheme of the $(Bz)_2Cr^+$ orbitals. The MO notation corresponds to that in $(Bz)_2Cr$.

$(Arene)_2Cr^+$

The MO diagram of the $(Bz)_2Cr^+$ cation (Fig. 5) differs from that of the neutral $(Bz)_2V$ molecule (Fig. 3). On going from $(Bz)_2V$ to $(Bz)_2Cr^+$ the valence-shell orbitals shift to lower energies by 5 - 6 eV. The $\alpha 1a_{1g}$-$\alpha 1e_{2g}$ separation increases while the $\alpha 1e_{1u}$-$\alpha 1a_{1g}$ energy difference decreases. Rydberg orbitals cannot be found among the lower-lying vacant MOs of the cation since its ionization energy is much higher than that of the neutral bisarene systems.

Table 4. TD DFT[a] / experimental[22,23,27,28] energies (eV) of selected $(Arene)_2Cr^+$ electronic states and the corresponding MO transitions.

State	Transition	$(Bz)_2Cr^+$	$(Tol)_2Cr^+$	$(Xyl)_2Cr^+$	$(Mes)_2Cr^+$
$^2E_{2g}$	$1e_{2g}\rightarrow 1a_{1g}$ d-d, MLCT	0.85(0.000)/ 1.05	0.83[b](0.000)/[c]	0.81[b](0.000)/[c]	0.77(0.000)/[c]
"$^4A_{2u}$"	$1e_{2g}\rightarrow 1e_{2u}$ MLCT	3.52(0.035)/ 3.71	3.47(0.036)/ 3.63	3.40(0.037)/ 3.55	3.31(0.038)/ 3.45
"$^2A_{1u}$" + "$^2E_{2u}$"	$1e_{2g}\rightarrow 1e_{2u}$ MLCT	4.25[b](0.000)/ 3.71	4.23 [b](0.000)/ 3.63	4.13 [b](0.001)/ 3.55	4.04[b](0.000)/ 3.45
"$^2A_{2u}$"	$1e_{2g}\rightarrow 1e_{2u}$ MLCT	4.87(0.219)/ 4.54	4.77(0.210)/ 4.35	4.66(0.200)/ 4.31	4.53(0.189)/ 4.25

[a] The calculated oscillator strengths are given in parentheses.

[b] An averaged energy and a sum of oscillator strengths is given for the components arising from state splitting.

[c] Experimental data are not available,

.

The TD DFT results (Table 4) demonstrate that very weak peak G observed in the near-IR absorption spectrum[22,23] of $(Bz)_2Cr^+$ arises from the $1e_{2g}\rightarrow 1a_{1g}$ d-d/MLCT transition. This assignment is in accord with that suggested on the basis of the SCF-X_α calculation.[31] Such interpretation is supported also by the photoelectron spectroscopy data.[58] The difference between the vertical ionization potentials corresponding to the detachment of the $1e_{2g}$ and $1a_{1g}$ electrons of neutral $(Bz)_2Cr$ is 1.01 eV. This value is equal to the energy of the $1e_{2g}\rightarrow 1a_{1g}$ vertical transition in the gas-phase $(Bz)_2Cr^+$ ion. The position of the G band in the experimental solution spectrum[22,23] (1.05 eV, Tables 1, 4) correlates, therefore, very well with the $1e_{2g}\rightarrow 1a_{1g}$ energy predicted by the photoelectron spectroscopy.

The strongest $1e_{2g}\rightarrow 1e_{2u}$ component ($A_{1g}\rightarrow A_{2u}$) is responsible for intense peak I observed in the experimental spectra of $(Arene)_2Cr^+$ at 4.25-4.24 eV (Table 4). The molar extinction of the longer-wavelength H band is close to that of peak I (Table 1). Band H should be assigned, therefore, to an allowed excitation. According to TD DFT, the only $(Bz)_2Cr^+$ transition with non-zero oscillator strength, lying below band I, is $^2A_{1g}\rightarrow$"$^4A_{2u}$", similar to $(Bz)_2V$. By analogy with peak E in the spectra of isoelectronic $(Arene)_2V$, band H should be assigned as a second component of the $1e_{2g}\rightarrow 1e_{2u}$ transition.

The $1e_{1u}\rightarrow 1a_{1g}$ excitation, suggested as a candidate responsible for peak H, [31] lies at 4.95 eV according to TD DFT. This energy exceeds the experimental value by 1.24 eV which makes such an assignment less probable. In contrast, the energies of the $1e_{2g}\rightarrow 1e_{2u}$ component considered (3.31-3.52 eV, Table 4) correlate well with the H band positions in the experimental

spectra (3.45-3.71 eV). However, the TD DFT calculations underestimate the H intensity which is predicted to be substantially lower than that for peak I (Table 4). Nevertheless, the TD DFT assignments appear to describe correctly the influence of the metal atom and ligand on the positions and relative intensities of electronic transitions in the bisarene systems studied.

Metal and ligand influence on the electronic excited states of (Arene)$_2$M (M = Cr, V, Cr$^+$)

The observed changes of excited-state parameters on going from one complex to another are reproduced by the TD DFT calculations not only for the Rydberg 4p transitions in (Bz)$_2$Cr and (Bz)$_2$V mentioned above. The differences in energies and intensities of valence-shell excitations can also be described by the computational results at the B3LYP/6-31++G(d,p) level of theory. For example, the $1e_{2g}\rightarrow 1a_{1g}$ band blue shift on going from (Bz)$_2$Cr$^+$ to (Bz)$_2$V is calculated to be 0.77 eV which agrees well with the experiment (0.66 eV, Tables 3, 4).

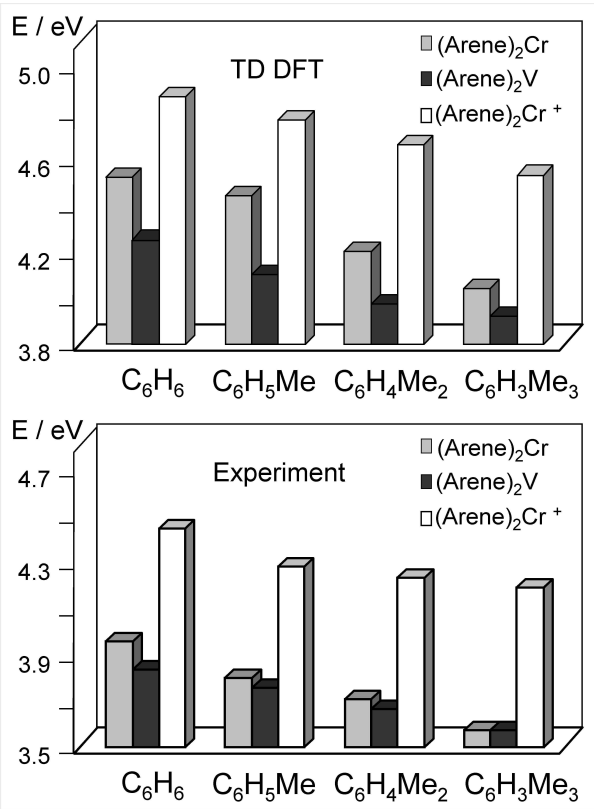

Fig.6. B3LYP/6-31++G(d,p) (top) and experimental[] (bottom) energies of the $A_{1g}\rightarrow A_{2u}$ component of the $1e_{2g}\rightarrow 1e_{2u}$ transition in (Arene)$_2$M (M=Cr, V, Cr$^+$).

The computed oscillator strength of the $A_{1g}\rightarrow A_{2u}$ transition responsible for the strong C, F and I bands increases by 83-145% on going from (Arene)$_2$Cr$^+$ to (Arene)$_2$V (Tables 3, 4). This trend correlates with the increase of the molar extinction coefficient when one goes from band I to peak F in the spectra of bisbenzene complexes (Table 1). On the other hand, the oscillator strength of the lower-lying $1e_{2g}\rightarrow 1e_{2u}$ component decreases from 0.035-0.038 in (Arene)$_2$Cr$^+$ to 0.012-0.13 in (Arene)$_2$V (Tables 3, 4). This computational result is in accord with the lower intensity of band E in the spectrum of (Bz)$_2$V as compared to band H in the spectrum of (Bz)$_2$Cr$^+$ (Table 1). The theoretical (Bz)$_2$Cr$^+$ / (Bz)$_2$V intensity ratio (2.9) is close to the experimental value (3.3). The decrease in the oscillator strength of the excitation considered can be explained by a larger separation of the corresponding level from the allowed "$^2A_{2u}$" state in the vanadium complexes (Fig. 4). As a result, the efficiency of the intensity transfer to the transition terminating at the "$^4A_{2u}$" state decreases on going from (Arene)$_2$Cr$^+$ to (Arene)$_2$V. The assignment of the C, F and I bands to the $A_{1g}\rightarrow A_{2u}$ component of the $1e_{2g}\rightarrow 1e_{2u}$ transition is supported by a good agreement between the predicted and observed trends of the peak position changes on going from one bisarene system to another. (Fig. 6). The TD DFT results reproduce both the experimental blue shift in the row (Arene)$_2$V - (Arene)$_2$Cr - (Arene)$_2$Cr$^+$ and the red shift caused by introduction of methyl groups into the ligands. The resulting TD DFT interpretations of the valence-shell absorption features in the spectra of (Arene)$_2$M are summarised in Table. 5.

Table 5. TD DFT assignment of the absorption features observed in the solution spectra[22-30] of (Arene)$_2$M (M = Cr, V, Cr$^+$).

M	Band[a]	Transition	Excited state
Cr	A	$1a_{1g}\rightarrow 2e_{1g}$ d-d, MLCT	$^1E_{1g}$
Cr	B[b]	$1e_{2g}\rightarrow 1e_{2u}$ MLCT	$^1A_{1u}$, $^1E_{2u}$
Cr	C	$1e_{2g}\rightarrow 1e_{2u}$ MLCT	$^1A_{2u}$
V, Cr$^+$	D, G	$1e_{2g}\rightarrow 1a_{1g}$ d-d, LMCT	$^2E_{2g}$
V, Cr$^+$	E,[b] H	$1e_{2g}\rightarrow 1e_{2u}$ MLCT	"$^2A_{1u}$" + "$^2E_{2u}$" or "$^4A_{2u}$"[c]
V, Cr$^+$	F, I	$1e_{2g}\rightarrow 1e_{2u}$ MLCT	"$^2A_{2u}$"[c]

[a] The band notation corresponds to that in Table 1.

[b] Vibronically allowed transitions from $1e_{2g}$ to $2e_{1g}$ and $2e_{2g}$ can also contribute to the B and E intensities.

[c] See text for the electronic state assignments.

Conclusions

The TD DFT study of twelve bisarene systems carried out in this work together with analysis of experimental spectroscopic data provides an interpretation of the features observed in the absorption spectra of (Arene)$_2$M (M=Cr, V, Cr$^+$) and an explanation of the changes in the spectra on varying the metal and ligand in a sandwich complex. Our calculations confirm a key role of Rydberg excitations in the gas-phase spectra of the neutral bisarene molecules. The computational results are in accord with the assignments of Rydberg structures made previously. [27,40-46] The computed scheme of Rydberg-valence configuration interactions in (Arene)$_2$Cr and (Arene)$_2$V reproduces the experimental observations.

TD DFT supports the interpretation[29,31] of the strong intravalency absorption band at 3.87, 4.00 and 4.54 eV in the

spectra of $(Bz)_2Cr$, $(Bz)_2V$ and $(Bz)_2Cr^+$, respectively, as the symmetry allowed component of the $1e_{2g}\rightarrow1e_{2u}$ excitation. The TD DFT transition energies demonstrate, however, that the $1e_{1u}\rightarrow1a_{1g}$ excitation cannot be responsible for the longer-wavelength bands E and H in the spectra of $(Bz)_2V$ and $(Bz)_2Cr^+$ as it has been suggested earlier.[30,31] These features should rather be considered as additional components of the $1e_{2g}\rightarrow1e_{2u}$ transition. Our calculations show that the red shift of an absorption feature on introduction of electron-donating groups to the ligand can not be a reliable basis for its interpretation as a LMCT excitation. The computed energies of the $1e_{2g}\rightarrow1e_{2u}$ MLCT components in $(Arene)_2M$ also decrease on methylation of arene ligands. For the lowest-energy peak in the spectra of $(Arene)_2V$, TD DFT suggests an assignment to the $1e_{2g}\rightarrow1a_{1g}$ excitation instead of $1a_{1g}\rightarrow2e_{1g}$.[30] The B3LYP/6-31++G(d,p) calculations describe correctly the absorption band shifts and intensity changes observed on going from one bisarene complex to another.

Acknowledgements

This work was supported by the Russian Science Foundation (Project 14-13-00832).

Notes and references

[a] *G.A. Razuvaev Institute of Organometallic Chemistry RAS Nizhny Novgorod 603950, Russian Federation. Fax: +7 8314627497; Tel: +7 8314627370; E-mail: sketkov@iomc.ras.ru*

[b] *Nizhny Novgorod State University, Nizhny Novgorod 603950, Russian Federation . Fax: +7 8314627497; Tel: +7 8314627370; E-mail: sketkov@iomc.ras.ru*

[c] *Institute of Atomic and Molecular Sciences, Academia Sinica, Taipei 10617, Taiwan*

† Electronic Supplementary Information (ESI) available: Comparison of the TD DFT results obtained in this work for $(Bz)_2Cr$ at various levels of theory. See DOI: 10.1039/b000000x/

1 (a) D. M. P. Mingos, in *Comprehensive Organometallic Chemistry*, ed. G. Wilkinson, F. G. A. Stone and E. W. Abel, Pergamon Press, Oxford, 1982, vol. 3, 1-88; (b) M. J. Morris, in *Comprehensive Organometallic Chemistry II*; ed. E. W. Abel, F. G. A. Stone and G. Wilkinson, Pergamon Press, Oxford, 1995, vol. 5, 471-549; (c) Ch. Elschenbroich, *Organometallics, 3rd, Completely Revised and Extended Edition*, Wiley-VCH: Weinheim, 2011; (d) D. Seyferth, *Organometallics*, 2002, **21**, 1520; (e) D. Seyferth, *Organometallics*, 2002, **21**, 2800.

2 Hegedus, L. S. *Transition metals in the synthesis of complex organic molecules*, University Science: California, 1994.

3 Omae, I. *Applications of organometallic compounds*; John Wiley & Sons: Wheinheim, 1998.

4 K. Muñiz, *Top. Organomet. Chem.*, 2004, **7**, 205.

5 J. Rigby and M. Kondratenkov, *Top. Organomet. Chem.*, 2004, **7**, 181.

5 D. Astruc, *Organometallic chemistry and catalysis*, Springer, Berlin, 2007.

6 J. Wang, P. H. Acioli, and J. Jellinek, *J. Am. Chem. Soc.* 2005, **127**, 2812.

7 A. Nakajima, *Bull. Chem. Soc. Jpn.*, 2013, **86**, 414.

8 J. Jiang, J. R. Smith, Y. Luo, H. Grennberg and H. Ottosson, *J. Phys. Chem. C*, 2011, **115**, 785.

9 X. Zhang and J. Wang, *J. Phys. Chem. A*, 2008, **112**, 296.

10 H. Xiang, J. Yang, J. G. Hou and Q. Zhu, *J. Am. Chem. Soc.*, 2006, **128**, 2310.

11 M. Mitsui, S. Nagaoka, T. Matsumoto and A. Nakajima, *J. Phys. Chem. B*, 2006, **110**, 2968.

12 K. Judai, M. Hirano, H. Kawamata, S. Yabushita, A. Nakajima and K. Kaya, *Chem. Phys. Lett*., 1997, **270**, 23.

13 T. Yasuike and S. Yabushita, *J. Phys. Chem. A*, 1999, **103**, 4533.

14 W. Zheng, J. M. Nilles, O. C. Thomas and K. H. Bowen, *Chem. Phys. Lett*., 2005, **401**, 266.

15 T. Kurikawa, H. Takeda, M. Hirano, K. Judai, T. Arita, S. Nagao, A. Nakajima and K. Kaya, *Organometallics*, 1999, **18**, 1430.

16 H. Liu, Q.-S. Li, Y. Xie, R. B. King, and H. F. Schaefer, *J. Phys. Chem. A*, 2011, **115**, 9022.

17 T. Masubuchi, K. Ohi, T. Iwasa and A. Nakajima, *J. Chem. Phys.*, 2012, **137**, 224305.

18 T. Zhang, Z. Tian, L. Zhu, X. Zhang, Q. Chen and J. Wang, *Comput. Theor. Chem.*, 2013, **1013**, 46.

19 J. Wang and J. Jellinek, *J. Phys. Chem. A*, 2005, **109**, 10180.

20 J. I. Martínez, J. M. García-Lastra, M. J. López and J. A. Alonso, *J. Chem. Phys.*, 2010, **132**, 044314.

21 V. M. Rayón and G. Frenking, *Organometallics*, 2003, **22**, 3304.

22 S. Yamada, H. Yamazaki, H. Nishikawa and R. Tsushida, *Bull. Chem. Soc. Japan*, 1960, **33**, 681.

23 R. D. Feltham, *J. Inorg. Nucl. Chem.*, 1961, **16**, 197.

24 D. R. Scott and R. S. Becker, *J. Phys. Chem.*, 1965, **69**, 3207.

25 D. A. Levy and L. E. Orgel, *Mol. Phys.*, 1961, **4**, 93.

26 K. D. Warren, *Structure and Bonding (Berlin)*, 1976, **27**, 45.

27 S. Y. Ketkov, *Ph.D. Thesis*, A.N. Nesmeyanov Institute of Organoelement Compounds, Moscow, 1988.

28 S. Y. Ketkov and G. A. Domrachev, Metalloorgan. Khimiya, 1992, **2**, 919.

29 M. P. Andrews, S. M. Mattar and G. A. Ozin, *J. Phys. Chem.*, 1986, **90**, 1037.

30 A. McCamley and R. N. Perutz, *J. Phys. Chem.*, 1991, **95**, 2738.

31 J. Weber, M. Geoffroy, A. Goursot and E. Penigault, *J. Am. Chem. Soc.*, 1978, **100**, 3995.

32 G.G. Tairova, E.F. Kvashina, O.N. Krasochka, G.A. Kichigina,Yu.A. Schvetsov, E.M. Lisetskii, L.O. Atovmyan, Yu.G. Borod'ko, *Nouv. J. Chim.*, 1981, **5**, 603.

33 (a) E. K. U. Gross, J. F. Dobson and M. Petersilka, *Top. Curr. Chem.*, 1996, **181**, 81; (b) M. E. Casida, in *Recent Advances in Density Functional Methods*, ed. D. E. Chong, World Scientific, Singapore, 1995, vol. 1, pp. 155-192; (c) R. Van Leeuwen, *Int. J. Mod. Phys. B*, 2001, **15**, 1969; (d) F. Trani, G. Scalmani, G. Zheng, I. Carnimeo, M. J. Frisch and V. Barone, *J. Chem. Theory Comput.*, 2011, **7**, 3304; (e) C.-L. Cheng, Q. Wu and T. V. Voorhis, *J. Chem. Phys.*, 2008, **129**, 124112; (f) M. E. Casida and M. Huix-Rotllant, *Annu. Rev. Phys. Chem.*, 2012, **63**, 287.

34 A. Rosa, G. Ricciardi, O. Gritsenko and E. J. Baerends, *Structure and Bonding*, 2004, **112**, 49.

35 J. P. Holland and J. C. Green, *J. Comput. Chem.*, 2010, **31**, 1008.

36 C. J. Cramer and D. G. Truhlar, *Phys. Chem. Chem. Phys.*, 2009, **11**, 10757.

37 Y. L. Li , L. Han , Y. Mei and J. Z. H. Zhang, *Chem. Phys. Lett*., 2009, **482**, 217;

38 T. A. Jackson, J. Krzystek, A. Ozarowski, G. B. Wijeratne, B. F. Wicker, D. J. Mindiola and J. Telser, *Organometallics*, 2012, **31**, 8265.

39 (a) P. Boulet, H. Chermette, C. Daul, F. Gilardoni, F. Rogemond, J. Weber and G. Zuber, *J. Phys. Chem. A*, 2001, **105**, 885; (b) U. Salzner, *J. Chem. Theory Comput.*, 2013, **9**, 4064.

40 G. A. Domrachev, S. Yu. Ketkov and G. A. Razuvaev, *J. Organomet. Chem.,*1987, **328**, 341.

41 S. Yu. Ketkov, G. A. Domrachev and G. A. Razuvaev, *J. Mol. Struct*., 1989, **195**, 175.

42 A. Penner, A. Amirav, *J. Chem. Phys.*, 1993, **99**, 176.

43 S. Yu. Ketkov, J. C. Green and C. P. Mehnert, *J. Chem. Soc., Faraday Trans., 1997*, **93**, 2461

44 S. Yu. Ketkov, G. A. Domrachev, C. P. Mehnert and J. C. Green, *Russ. Chem. Bull.,* 1998, **47**, 868

45 S. Yu. Ketkov, in *Multiphoton and Multielectron Driven Processes in Organics: New Phenomena, Materials and Applications*, ed. F. Kajzar and V. M. Agranovich, Kluwer Academic Publishers, Dordrecht, 2000, 503-512.

46 S. Yu. Ketkov, in *Trends in Organometallic Chemistry Research*, ed. M. A. Cato, Nova Science, New York, 2005, 187-207.
47 S. Yu. Ketkov, H. L. Selzle, E. W. Schlag, *J. Chem. Phys.*, 2004, **121**, 149.
48 S. Y. Ketkov, *J. Organomet. Chem.*, 1992, **429**, C38.
49 S. Y. Ketkov, *Russ. Chem. Bull.*, 1999, **48**, 1656.
50 M. J. Frisch, G. W. Trucks, H. B. Schlegel, G. E. Scuseria, M. A. Robb, J. R. Cheeseman, G. Scalmani, V. Barone, B. Mennucci, G. A. Petersson, H. Nakatsuji, M. Caricato, X. Li, H. P. Hratchian, A. F. Izmaylov, J. Bloino, G. Zheng, J. L. Sonnenberg, M. Hada, M. Ehara, K. Toyota, R. Fukuda, J. Hasegawa, M. Ishida, T. Nakajima, Y. Honda, O. Kitao, H. Nakai, T. Vreven, J. A. Montgomery, Jr., J. E. Peralta, F. Ogliaro, M. Bearpark, J. J. Heyd, E. Brothers, K. N. Kudin, V. N. Staroverov, R. Kobayashi, J. Normand, K. Raghavachari, A. Rendell, J. C. Burant, S. S. Iyengar, J. Tomasi, M. Cossi, N. Rega, J. M. Millam, M. Klene, J. E. Knox, J. B. Cross, V. Bakken, C. Adamo, J. Jaramillo, R. Gomperts, R. E. Stratmann, O. Yazyev, A. J. Austin, R. Cammi, C. Pomelli, J. W. Ochterski, R. L. Martin, K. Morokuma, V. G. Zakrzewski, G. A. Voth, P. Salvador, J. J. Dannenberg, S. Dapprich, A. D. Daniels, O. Farkas, J. B. Foresman, J. V. Ortiz, J. Cioslowski and D. J. Fox, *Gaussian, Inc.*, Wallingford CT, 2009.
51 A. D. Boese and N. C. Handy, *J. Chem. Phys.*, 2001, **114**, 5497.
52 J. P. Perdew, K. Burke, and Y. Wang, *Phys. Rev. B*, 1996, **54**, 16533.
53 A. D. Becke, *J. Chem. Phys.*, 1993, **98**, 5648.
54 (a) W. J. Hehre, R. Ditchfield and J.A. Pople, *J. Chem. Phys.*, 1972, **56**, 2257; (b) M. M. Francl, W. J. Petro, W. J. Hehre, J. S. Binkley, M. S. Gordon, D. J. DeFrees and J. A. Pople, *J. Chem. Phys*., 1982, **77**, 3654; (c) V. Rassolov, J.A. Pople, M. Ratner and T.L. Windus, *J. Chem. Phys.*, 1998, **109**, 1223; (d) R. Krishnan, J. S. Binkley, R. Seeger and J. A. Pople, *J. Chem. Phys*., 1980, **72**, 650; (e) P. J. Hay, *J. Chem. Phys*., 1977, **66**, 4377; (f) A. Schaefer, C. Huber, and R. Ahlrichs, *J. Chem. Phys*., 1994, **100,** 5829.
55 (a) N. C. Schiødt, R. Sessoli and F. C. Krebs, *Inorg Chem.*, 2004, **43**,1986; (b) B. Morosin, *Acta Cryst,*, 1974, **B30**, 838; (c) K. A. Lyssenko, A. A. Korlyukov, D. G. Golovanov, S. Yu. Ketkov and M. Yu. Antipin, *J. Phys. Chem. A*, 2006, **110**, 6545; (d) A. Haaland, *Acta Chem. Scand*., 1965, **19**, 41; (e) E. O. Fischer, H. P. Fritz, J. Manchot, E. Priebe and R. Schneider, *Chem. Ber.*, 1963, **96**, 1418; (f) D. Braga and P. Sabatino, *Acta Cryst.*, 1990, C**46**, 2308.
56 (a) R. Sahnoun and C. Mjoule, *J. Phys. Chem. A*, 2001, **105,** 6176; (b) H. Xiang, J. Yang, J. G. Hou, and Q. Zhu, *J. Am. Chem. Soc.*, 2006, **128,** 2310; (c) T. Strassner and M. A. Taige, *J. Chem. Theory Comput*., 2005, **1,** 848; (d) A. Perrier, D. Gourier, L. Joubert, and C. Adamo, *PCCP,* 2003*,* **5,** 337; (e) R. Pandey, B. K. Rao, B. P. Jena, and M. A. Blanco*, J. Am. Chem. Soc*.,2001, **123,** 3799; (f) A. Berces and T. Ziegler, *J. Phys. Chem.*, 1994, **98,** 13233.
57 S. Yu. Ketkov and H. L. Selzle, *Z. Phys. Chem.*, 2007, **221**, 597.
58 (a) J. C. Green, *Structure and Bonding*, 1981, **43**, 37, and the references cited therein; (b) M. F. Ryan, D. E. Richardson, D. L. Lichtenberger and N. E. Gruhn, *Organometallics,* 1994, **13**, 1190.
59 G. Herzberg, *Molecular Spectra and Molecular Structure. III. Electronic Spectra and Electronic Structure of Polyatomic Molecules*, Krieger, Malabar, 1991.